

# Partitioning of a Hybrid Lipid in Domains of Saturated and Unsaturated Lipids in a Model Cellular Membrane

Prashant Hitaishi, Priya Mandal, and Sajal K. Ghosh\*

Cite This: <https://doi.org/10.1021/acsomega.1c04835>

Read Online

ACCESS |



Metrics &amp; More



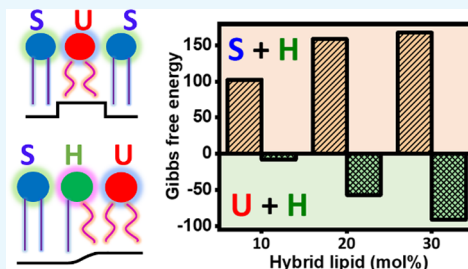
Article Recommendations



Supporting Information

**ABSTRACT:** The cellular membranes are composed of hundreds of components such as lipids, proteins, and sterols that are chemically and physically distinct from each other. The lipid–lipid and lipid–protein interactions form domains in this membrane, which play vital roles in membrane physiology. The hybrid lipids (HLs) with one saturated and one unsaturated chain can control the shape and size of these domains, ensuring the thermodynamic stability of a membrane. In this study, the thermodynamics of mixing of a HL and its structural effects on the phase separated domains in a model membrane composed of a saturated and an unsaturated lipid have been investigated. The HL is observed to mix into an unsaturated lipid reducing the Gibbs free energy, whereas the mixing is unfavorable in a saturated lipid. The presence of an HL in an unsaturated lipid tends to increase its area fraction, which is reflected in the enhanced correlation length across the bilayers in a multilayered sample. There is a feeble effect on the domain structure of the saturated lipid due to the presence of the HLs at the phase boundary. This study concludes that the HLs preferentially participate in the unsaturated lipid regions compared to that of a saturated lipid.

**KEYWORDS:** phase separation, hybrid lipids, lipid membrane, X-ray scattering, isotherm, Gibbs free energy



S: Saturated lipid, U: Unsaturated lipid, H: Hybrid lipid

## 1. INTRODUCTION

The modern research in the cellular membrane started with the “fluid mosaic model” assuming it as a homogeneous matrix of various lipids in which different proteins and the lipids float and diffuse freely in two dimensions.<sup>1</sup> Further development and research considered the concept of heterogeneity, proposing the “mattress model” in 1984.<sup>2</sup> In 1997, Simons and Ikonen first coined the term “rafts” to define the lateral heterogeneity in the lipid membranes.<sup>3</sup> These rafts are highly dynamic small liquid-ordered ( $L_o$ ) domains formed in the plasma membrane with a high concentration of cholesterol and glycosphingolipids compared to the rest portion of the membrane.<sup>4–6</sup> These rafts ensure a favorable and selective environment for various biological phenomena, such as signal processing, active sites for lipid–lipid interactions, a platform for lipid–protein interactions, pathogen binding, and genetically modified diseases.<sup>7,8</sup> They also protect the membrane against adverse environmental conditions.<sup>9</sup>

Over the last three decades, there have been immense theoretical works in understanding the thermodynamics of raft formation and its stability in a cellular membrane. The domains in a model membrane can be understood as the phase separation of saturated and unsaturated lipids when they are allowed to form a self-assembled structure. The domains appear due to positive line tension at the interfaces of lipids because of hydrophobic mismatch between the hydrocarbon chains of varying lengths.<sup>10</sup> The shape of a domain is governed

by a competition between line tension favoring a compact circular shape and the long-range electrostatic dipolar repulsion preferring a noncircular shape.<sup>11</sup> While for a relatively weaker line tension, the system entropy dominates to form nanodomains, a stronger line tension decreases the length of total phase boundary to form a microdomain.<sup>12</sup> Theoretical models have also predicted the line tension to drive a budding process in a flat or weakly curved domain.<sup>13</sup>

A hybrid lipid (HL) with one saturated and one unsaturated chain can act as a line-active molecule to control the strength of line tension at the interface of a saturated and an unsaturated lipid to stabilize a domain. In the absence of such an HL or any other stabilizing agent, smaller domains may coalesce to form a larger one.<sup>14,15</sup> For example, the 1-palmitoyl-2-oleoyl-*sn*-glycero-3-phosphocholine (POPC) is such an HL that can assemble in a preferred orientation at the interface of saturated 1,2-dipalmitoyl-*sn*-glycero-3-phosphocholine (DPPC) and unsaturated 1,2-dioleoyl-*sn*-glycero-3-phosphocholine (DOPC) to form a domain of a smaller size. However, in the case of the DPPC/DOPC/cholesterol system,

Received: September 2, 2021

Accepted: November 30, 2021

domain size is reported to increase with cholesterol concentration to a much larger size.<sup>16</sup> Note that the higher the degree of unsaturation in an HL is, the greater is the reduction in the interfacial line tension.<sup>17</sup> The domain formation in mixed lipid monolayers at the air–water interface<sup>11</sup> and vesicles are studied extensively using various microscopic<sup>8,18–23</sup> and NMR techniques<sup>24,25</sup> Even electron paramagnetic resonance<sup>26</sup> and X-ray and neutron scattering techniques have been employed for the purpose.<sup>27</sup> The effect of compression rate, pressure, and time on the shape of domains formed in monolayer at the air–water interface has been studied using a Brewster angle microscope.<sup>28,29</sup> A detailed review in the field can be found in ref 30. All these studies hypothesize that a model membrane with a saturated lipid, cholesterol, and hybrid lipid could be a better system to mimic a biological membrane, as they form nanodomains. This would be a preferred membrane compared to the one with a saturated lipid, cholesterol, and unsaturated lipid that form a micro-domain.

As mentioned above, there are numerous theoretical studies on the role of an HL in controlling the size of a domain in a multicomponent lipid membrane. Though there are a few experimental studies, the results require considerable clarifications. While Szekely et al. quantified the linactant nature of an HL in a mixture of saturated and unsaturated lipid,<sup>31</sup> Shimokawa et al. explained that POPC does not behave as a linactant in a four-component system composed of DPPC, DOPC, POPC, and cholesterol.<sup>32</sup> Further, the comprehension of preferential distribution of the HLs in and around a saturated and an unsaturated domain demands a more careful experimental study. Therefore, in the present paper, two approaches, namely, the measurements of the area–pressure isotherm of the lipid monolayer and the X-ray reflectivity study of lipid multilayers, have been utilized to figure out the thermodynamics of mixing and structural effects of HL in a model cellular membrane composed of a saturated and an unsaturated lipid.

## 2. MATERIALS AND METHODS

**2.1. Materials.** Zwitterionic lipids 1,2-dipalmitoyl-*sn*-glycero-3-phosphocholine (DPPC), 1,2-dioleoyl-*sn*-glycero-3-phosphocholine (DOPC), and 1-palmitoyl-2-oleoyl-*sn*-glycero-3-phosphocholine (POPC) were purchased from Avanti Polar Lipids (Alabaster, AL) in powder form and were used without further purification. The molecular structures of the lipids used in the study are shown in Figure 1. The spectroscopic grade chloroform was purchased from Sigma Aldrich (USA), and 2,2,2-trifluoroethanol (TFE) was from Tokyo Chemical Industry (Japan). Deionized (DI) (Milli-Q, Millipore) water with resistivity  $\sim 18 \text{ M}\Omega\cdot\text{cm}$  and pH  $\sim 8.5$  was used throughout the experiment. The silicon (100) wafer with one side having a polished surface was purchased from Waferpro.

**2.2. Methods.** **2.2.1. Surface Pressure–Area Isotherms of Lipid Monolayers.** A Langmuir trough of size  $56 \times 15 \times 0.25 \text{ cm}^3$  (Apex, India) with two symmetric Teflon barriers and a Wilhelmy balance has been used for experiments on a lipid monolayer formed at the air–water interface. To study the physical and thermodynamic properties of a monolayer, surface pressure–area isotherms were recorded at room temperature ( $\sim 25 \text{ }^\circ\text{C}$ ) for various lipid mixtures. Measured quantities of powder lipids were dissolved in chloroform to obtain the certain mole percent (mol %) of a component following the

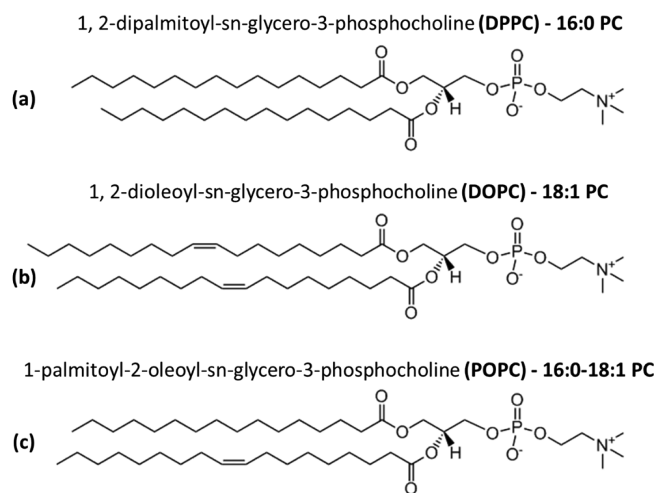


**Figure 1.** Chemical structures of all three lipids used: (a) saturated lipid DPPC, (b) unsaturated lipid DOPC, and (c) hybrid lipid POPC.

expression  $X_A = \frac{x/M_A}{x/M_A + y/M_B + z/M_C} \times 100\%$ , where  $X_A$  is the mol % of lipid component A. Here, X, Y, and Z are the measured quantities of components A, B, and C with their respective molecular weights  $M_A$ ,  $M_B$ , and  $M_C$ . A 100  $\mu\text{L}$  solution of final concentration of 0.5 mg/mL was spread over the water surface using a Hamilton micro syringe. Then, we waited for 20 min to allow the complete evaporation of the solvent. Monolayers were compressed at a constant rate of 6 mm/min until the collapse pressure was reached.

**2.2.2. X-ray Reflectivity Measurements of Lipid Multilayers.** For depositing lipid multilayers, polished Si substrates (100) of size  $10 \times 15 \text{ mm}^2$  were used after cleaning by bath sonication using two alternate cycles, each of 15 min, in methanol and DI water. Then, the substrates were dried under gentle  $\text{N}_2$  flow, and they were exposed to UV radiation for 30 min at  $50 \text{ }^\circ\text{C}$  to make them hydrophilic. The powder lipids were dissolved in a solution of a mixture of chloroform and TFE (1:1, v/v) to obtain the highly oriented stacks of lipid bilayers on a hydrophilic Si substrate.<sup>33,34</sup> A 50  $\mu\text{L}$  lipid solution of final concentration of 5 mg/mL was drop-cast on the substrate using a Hamilton micro syringe followed by the rock and roll method.<sup>33–35</sup> For the slow evaporation of solvent, the samples were then kept in a fume hood for 2 h, and later, they were taken in a vacuum chamber for 24 h. It ensured the complete removal of any traces of solvent. They were then preserved for 36 h at  $50 \text{ }^\circ\text{C}$  in a sealed glass Petri dish in an environment of saturated salt solutions of KCl,  $\text{KNO}_3$ , and  $\text{K}_2\text{SO}_4$  to maintain a relative humidity (RH) of 85, 95, and 98%, respectively.

X-ray reflectivity (XRR) experiments were carried out using an in-house X-ray instrument (Bruker, Discover D8) equipped with Cu  $K\alpha$  tube with a wavelength ( $\lambda$ ) of  $1.54 \text{ \AA}$ . A circular beam of diameter 1 mm was used for the scattering experiment. A specially designed sealed sample chamber with a reservoir storing the saturated salt solution was used to maintain certain thermodynamic conditions. The scattered X-rays from samples were collected by a point detector as a function of the incidence angle ( $\theta_i$ ) at the specular condition keeping the angle of reflection ( $\theta_r$ ) the same as the incident one. Data were collected for each sample at three different RHs, namely, 85, 95, and 98%, for implementing the swelling method to extract the electron density profile of a bilayer.<sup>36,37</sup>

The interbilayer spacing ( $d$ -spacing) was calculated from  $d = \frac{2\pi}{q_z}$  by applying Bragg's law,  $q_z = \frac{4\pi}{\lambda} \sin \theta_i$ . This  $q_z$  is the  $z$ -component of the wave vector transfer where the  $z$ -direction is along the normal of the stacks of bilayer lying horizontally on the Si-substrate.

### 3. RESULTS AND DISCUSSIONS

Two model membranes, one being the lipid monolayer formed at the air–water interface and the other being the lipid multilayers formed on a hydrophilic Si-substrate, have been utilized to quantify the participation of a hybrid lipid in the gel and fluid phases of a saturated and an unsaturated lipid, respectively. The complementary techniques of isotherm measurements and X-ray reflectivity study have shed light on this purpose and are explained in the following sections.

**3.1. Measurements of the Surface Pressure–Area ( $\pi$ – $A$ ) Isotherm.** The pressure ( $\pi$ )–area ( $A$ ) isotherm measurement is an effective and important technique to study the interaction among amphiphilic molecules by quantifying the thermodynamic parameters.<sup>29,38–47</sup> DPPC (16:0 PC) is a saturated lipid with a main phase transition temperature ( $T_m$ ) of  $\sim 41$  °C.<sup>48</sup> Below this temperature, these lipids self-assemble into a bilayer in bulk water forming a gel or solid phase where the acyl chains are tightly packed with a conformationally ordered state. Because of the amphiphilic nature, they also form a monolayer at the air–water interface projecting their hydrophobic chains into the air and attaching the hydrophilic heads to water. This monolayer undergoes various phases on compression depending upon the available area to each molecule at a given temperature. These phases are characterized by the change in slope of the surface pressure ( $\pi$ )–area ( $A$ ) isotherm. Initially, when the barriers are far apart, each molecule occupies a large area with a negligible intermolecular interaction, giving rise to a gaseous phase. On compression, the lipid film forms the liquid extended (LE) phase, characterized by a considerable intermolecular interaction. Further compression constructs a compact film of the liquid condensed (LC) phase that may finally collapse at very low available area per molecule. For the DPPC lipids, there is an intermediate region of coexisting LE and LC phases exhibiting a first order phase transition, which is characterized by a plateau in the isotherm (Figure 2a). As shown in Figure 1, DOPC (18:1 PC) is an unsaturated lipid with a  $T_m$  of  $\sim -20$  °C<sup>48</sup> that exhibits gaseous, LE and LC phases in its monolayer film without any coexisting region of LE–LC phases (Figure

2a). The hybrid lipid POPC (16:0–18:1 PC) with a  $T_m$  of  $\sim -2$  °C<sup>48</sup> shows an isotherm that is qualitatively similar to that of the DOPC lipid. Because of floppy and disordered chains, the steric repulsion among the DOPC lipids is much higher than that of the DPPC with ordered chains. Therefore, the unsaturated DOPC occupies more area compared to the saturated DPPC. As evident in Figure 2, at a given surface pressure, the hybrid lipid POPC with one saturated and another unsaturated chain possesses an area that is intermediate of DOPC and DPPC. The in-plane elasticity ( $E$ ) of a lipid film is evaluated using the relation

$$E = -A \left( \frac{\partial \pi}{\partial A} \right)_T \quad (1)$$

Here the mean molecular area is denoted with  $A$ , whereas  $\pi$  is the in-plane pressure at a given temperature ( $T$ ).<sup>38,49,50</sup> As shown in the inset of Figure 2, the elasticity exhibits a much higher value for DPPC compared to other lipids in the LC phase, explaining the compact structure of the DPPC film. However, the value is lower than the unsaturated lipids at  $\pi < 15$  mN/m probably due to the weaker steric repulsion among the saturated lipids in the LE phase, which makes the film easier to compress.

As depicted in Figure 2a, the isotherm of the mixed lipid system, at 50/50 mol % of DPPC and DOPC, does not show any coexistence region; rather, it exhibits a continuous transition, which has also been reported earlier.<sup>29</sup> The nature of the isotherm is quite similar to the unsaturated DOPC with an intermediate area/molecule. Interestingly, the addition of POPC in the mixed system shifts the isotherm toward the isotherms of the unsaturated lipid. The increased lift-off area of the mixed system in the presence of POPC suggests the enhanced repulsive intermolecular interaction. This repulsion in the ternary DPPC/DOPC/POPC system causes the film to become harder to compress and provides a slightly increased value of the in-plane elasticity compared to the binary DPPC/DOPC system (inset of Figure 2a).

The excess Gibbs free energy ( $\Delta G_{\text{exc}}$ ) is calculated from the isotherms using eq 2, as follows:

$$\Delta G_{\text{exc}} = \int_0^\pi [A_{12} - (\chi_1 A_1 + \chi_2 A_2)] d\pi \quad (2)$$

where  $A_{12}$  is the mean molecular area observed in the monolayer of a binary system.<sup>38,49,50</sup>  $A_1$  and  $A_2$  are the mean molecular area of lipids observed in the respective isotherms of monolayer of each individual component. Note that  $\chi_1$  and  $\chi_2$  are the mole fractions of the components taken to form a binary system. This excess Gibbs free energy ( $\Delta G_{\text{exc}}$ ) for the mixed DPPC/DOPC system is positive, showing an unfavorable interaction among the components. It arises due to the mismatch of hydrocarbon chain lengths and their conformation as explained elsewhere.<sup>16,29,51–53</sup> It gives rise to the domain formation of one lipid in the matrix of the other. Interestingly, the presence of POPC in the mixed system brings down the value of ( $\Delta G_{\text{exc}}$ ) considerably (Figure 2b). In case of this ternary system, the effect of POPC has been investigated on the isotherm of the DPPC/DOPC mixture. Therefore, in eq 2,  $A_1$  is the mean area occupied by a molecule in the DPPC/DOPC system, while  $A_{12}$  is the mean area occupied by a molecule in the DPPC/DOPC/POPC system. The lower value of  $\Delta G_{\text{exc}}$  suggests that the hybrid lipid might promote the mixing of saturated DPPC and unsaturated

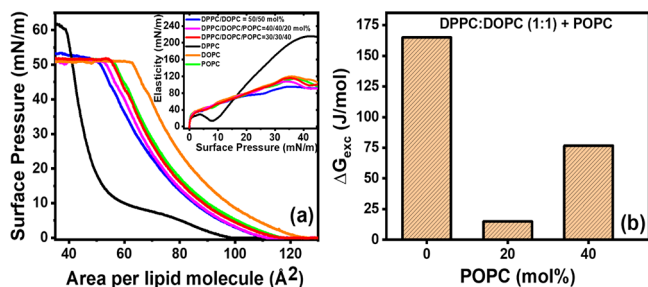


**Figure 2.** (a) Surface pressure–area isotherms of mixed lipid monolayers with added hybrid lipid POPC. The inset exhibits the corresponding in-plane elasticity of the lipid films. (b) Excess Gibbs free energy calculated over a pressure range of 0 to 45 mN/m. All the measurements were done at 25 °C.

DOPC in the monolayer system. However, it may also preferentially participate in one of the domains formed by these saturated and unsaturated lipids.

The mixing or participation of POPC in the DPPC and DOPC lipid monolayers has been investigated, and the measured isotherms are shown in Figure 3. The isotherm of

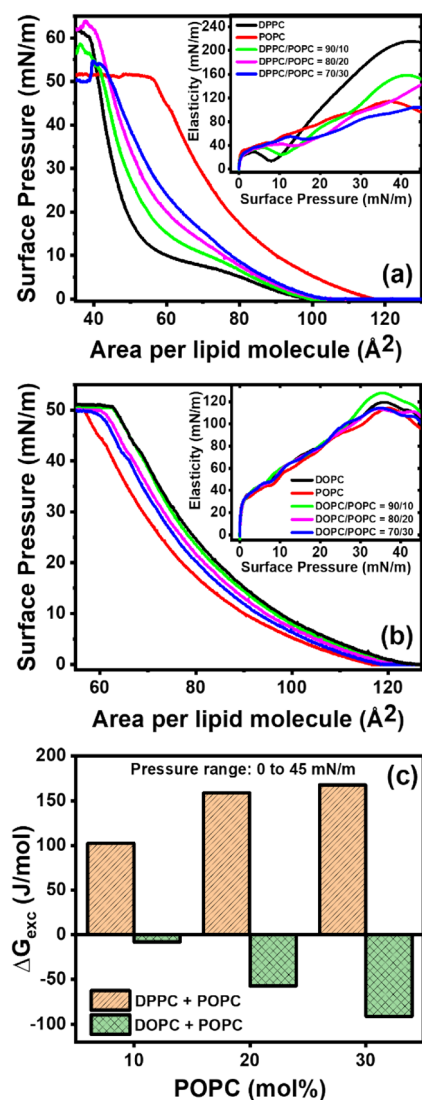


**Figure 3.** (a) Surface pressure–area isotherms of mixed lipid monolayers with an increased mol % of POPC concentration in (a) DPPC and (b) DOPC. Insets exhibit the corresponding 2D isothermal elasticity. (c) Excess Gibbs energy for the pressure range of 0 to 45 mN/m.

the DPPC/POPC binary system shifts toward the isotherm of pure POPC with an increase of lift-off area compared to the pure DPPC monolayer. The prominent co-existence region observed in the DPPC system diminishes with the addition of POPC, and the dip in in-plane elasticity curve corresponding to the coexistence region shifts toward higher pressure.<sup>54</sup> At a surface pressure of 30 mN/m, the elasticity of DPPC monolayer decreases significantly due to the presence of POPC. All these observations suggest the enhanced disorder nature of the overall film. The calculated positive values of  $\Delta G_{\text{exc}}$  shown in Figure 3c clearly exhibit that the interaction of POPC with DPPC is highly unfavorable and they do not mix

well into each other. Rather, POPC could phase separate out in the matrix of the DPPC monolayer. Note that, in this binary system, the effect of POPC has been investigated on the isotherm of DPPC. Therefore, in eq 2,  $A_1$  is the area occupied by a DPPC molecule, while  $A_{12}$  is the mean area occupied by a molecule in the DPPC/POPC system. The overall increase in the disorder nature of the film arises due to the presence of these domains of POPC. Note that the measurements are done at 25 °C, which is above the main phase transition temperature of POPC and below DPPC. In fact, Shimokawa et al. have reported the phase-separated domains in giant unilamellar vesicles (GUVs) in mixed DPPC/POPC investigated by a confocal microscope.<sup>32,55</sup> Our present study sheds light on the overall lipid film with respect to its in-plane elasticity and Gibbs free energy of mixing.

The  $\pi$ - $A$  isotherm of the binary DOPC/POPC system is shown in Figure 3b. The lift-off area of DOPC is slightly higher than that of the POPC lipids. Because of the two unsaturated chains in DOPC, the degree of disorder is more compared to POPC having one unsaturated chain. Therefore, the intermolecular steric repulsion would be higher in DOPC that leads to a higher area/molecule. With the addition of 10, 20, and 30 mol % of POPC in the DOPC, the isotherm of DOPC shifts toward the isotherm of POPC. The lift-off area of DOPC decreases from  $\sim 126$  to  $119 \text{ \AA}^2$ , suggesting a lesser repulsion among the mixed lipid system. Like the individual isotherm, the mixed system also shows a continuous phase transition. The Gibbs free energy of mixing for this binary system calculated from the isotherms is shown in Figure 3c. The negative value suggests a preferable mixing of these two components, which arises because of the attractive interaction between the components.

The macro phase separation in the DPPC/POPC system, the mixing of POPC in DOPC, and the phase behavior exhibited by the isotherms, along with the nature of interaction between DPPC-POPC and DOPC-POPC, depict that, at room temperature, POPC behaves like an unsaturated lipid having a behavior quite similar to DOPC. The authors of ref 32 predicted a similar behavior of POPC in a binary system. However, in a ternary system, they assumed it to be localized at the boundary of domains acting as a linactant. In our present study, as the mole percentage of the added hybrid lipid is high in the ternary system, the effect of the presence of the lipid at the boundary may be overshadowed by its presence in the bulk of the DOPC phase.

**3.2. X-ray Reflectivity (XRR) Study of Lipid Multilayers.** The X-ray reflectivity (XRR) experiment on a lipid multilayer formed on a substrate is a well-known technique to explore the structural details of a model cellular membrane in the presence of sterols, peptides, etc.<sup>33–37,56–62</sup> It provides multiple diffraction peaks due to the correlation among the bilayers stacked on top of each other along the substrate normal, forming a smectic liquid crystalline phase. Because of phase separated domains in the DPPC/DOPC binary system, two sets of equidistant Bragg peaks are observed in the XRR profile at room temperature.<sup>62–64</sup> In the present study, the sets are shown in Figure 4a; the first set of peaks observed at lower  $q_z$  exhibiting higher interbilayer separation ( $d$ -spacing) corresponds to the gel phase formed mainly by the DPPC lipids, whereas the second set of peaks represents the fluid phase formed dominantly by the unsaturated DOPC lipid. The  $d$ -spacings for the gel and fluid phases are calculated to be  $61.27 \pm 0.42$  and  $51.60 \pm 0.3 \text{ \AA}$ , respectively, at an RH of 85%,

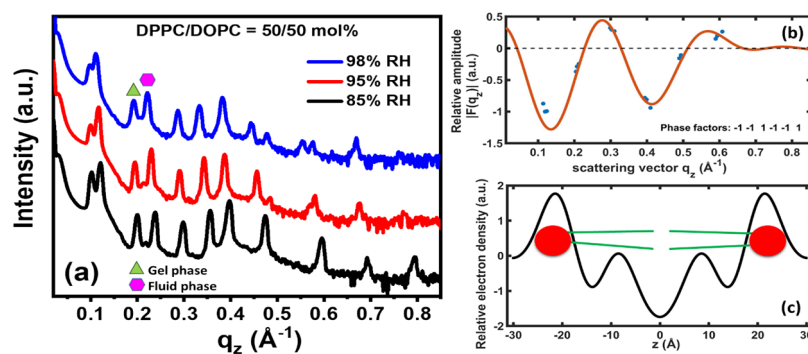


**Figure 4.** (a) X-ray reflectivity (XRR) data for a DPPC/DOPC (50/50) binary lipid system obtained from a stack of lipid bilayers on a Si substrate, measured at different relative humidities (RHs) at room temperature. The sets of equidistant Bragg peaks obtained due to correlation among the individual bilayers forming a one-dimensional crystalline arrangement along the normal of the substrate. (b) An illustration of the determination of phase factors by applying the swelling method on data shown in (a). Here, blue circles denote the form factor amplitude and the solid red line denotes the continuous form factor. (c) Electron density profile (EDP) corresponding to the gel phase of the binary system along with a schematic of the lipid molecule to relate the corresponding region of a lipid bilayer.

which increase by a few Å at higher RH. Note that these values are lower than the  $d$ -spacing reported for the multilamellar vesicles (MLVs) in bulk water.<sup>65</sup> In case of MLVs, the bilayers can swell apart due to interbilayer steric repulsion arising from the thermal undulation of the bilayers, which is partially restricted in case of a multilayer sample on a solid substrate at lower RH.

On addition of POPC in the DPPC/DOPC system, again two sets of lamellar peaks are observed as shown in Figure 5.

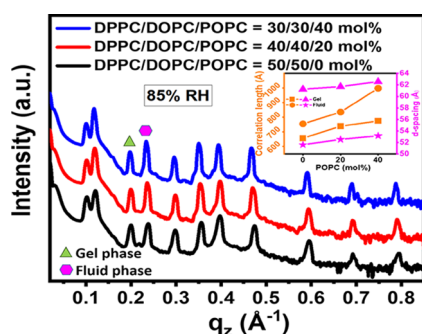


**Figure 5.** X-ray reflectivity (XRR) data of the DPPC/DOPC/POPC system in the presence of 0, 20, and 40 mol % of POPC at 85% relative humidity (RH). Correlation length and  $d$ -spacing calculated at 85% RH are shown in the inset.

Interestingly, the  $d$ -spacings for both the DPPC dominated gel phase and DOPC dominated fluid phase slightly increase (inset of Figure 5). As evident from the monolayer measurements, one saturated chain of POPC, which mixes well in DOPC, may decrease the disorder nature of DOPC lipid chains, providing a slight increase in bilayer thickness leading to a higher  $d$ -spacing. If POPC lipids were mixed in the DPPC domains, the bilayer thickness would have decreased due to the disorder conformation of the lipid chains. On the other hand, if POPC does not mix into DPPC, which is suggested by the positive Gibbs free energy measurement, there should have been no direct structural effect on the DPPC domains. However, even for this DPPC phase, we see a slight increase in the  $d$ -spacing. Actually, the presence of POPC in DOPC and at the phase boundary may increase the lateral pressure in the bilayer, which may cause a decrease in the chain tilt in the DPPC lipid, producing a little increase in the bilayer

thickness. Such a hypothesis of decrease in chain tilt demands a more careful and systematic study. Note that Szekely et al. have reported the two sets of Bragg peaks in MLVs of the binary DPPC/POPC system in the presence of  $\text{CaCl}_2$  into the solution.<sup>31</sup> Even though we could explain the preferential participation of the POPC into the DOPC domain in the present study, the  $d$ -spacing cannot provide an exact description of the structural organization of the lipids into a bilayer. Therefore, we have extended this work to extract the electron density profiles of each bilayer with different lipid compositions, which are described below.

To obtain the electron density profile (EDP), the swelling method has been implemented<sup>56,58–61,66–68</sup> on the data collected at different relative humidities (RHs) of 85, 95, and 98%. These different RHs alter the interbilayer spacing slightly, keeping the structure of the individual bilayer intact. Therefore, the diffraction peaks corresponding to a certain phase may shift to a lower  $q_z$  at higher RH. In this method, the form factor of the bilayer is assumed to be unaltered. Figure 4b illustrates the phasing of the gel phase of the DPPC lipid in the DPPC/DOPC mixed system. The solid blue circles denote the amplitude of the form factor that is directly related to the integrated intensity of Bragg peaks. This integrated intensity is modified by using a Lorentz correction factor, and due to the mirror plane symmetry of a bilayer, the phase factors are reduced to  $\pm 1$ .<sup>56,58,60</sup> A MATLAB code has been used to fit each peak using a Gaussian function to obtain the integrated intensity of the peak and further analyzed to obtain the continuous form factor.<sup>58</sup> Finally, these phase factors and the form factor are utilized to obtain the electron density profile (EDP) from ref 65 as shown in eq 3:

$$\rho_{\text{relative}}(z) = \frac{2}{d} \sum_n \nu(n) n \sqrt{I_n} \cos\left(\frac{2\pi n z}{d}\right) \quad (3)$$

Here,  $\nu(n)$  is the phase factor and  $I_n$  is the integrated intensity of  $n$ th order diffraction peak with  $d$  being the interbilayer spacing. Figure 4c shows the electron density profile (EDP) of the gel phase plotted in the arbitrary unit where the two maxima represent the two head-group regions of lipid molecules in two leaflets of a bilayer. The head-group regions have high electron density relative to the hydrocarbon chain region; hence, there is a minimum at  $z = 0$  Å that corresponds to the center of the bilayer. Here, the electron

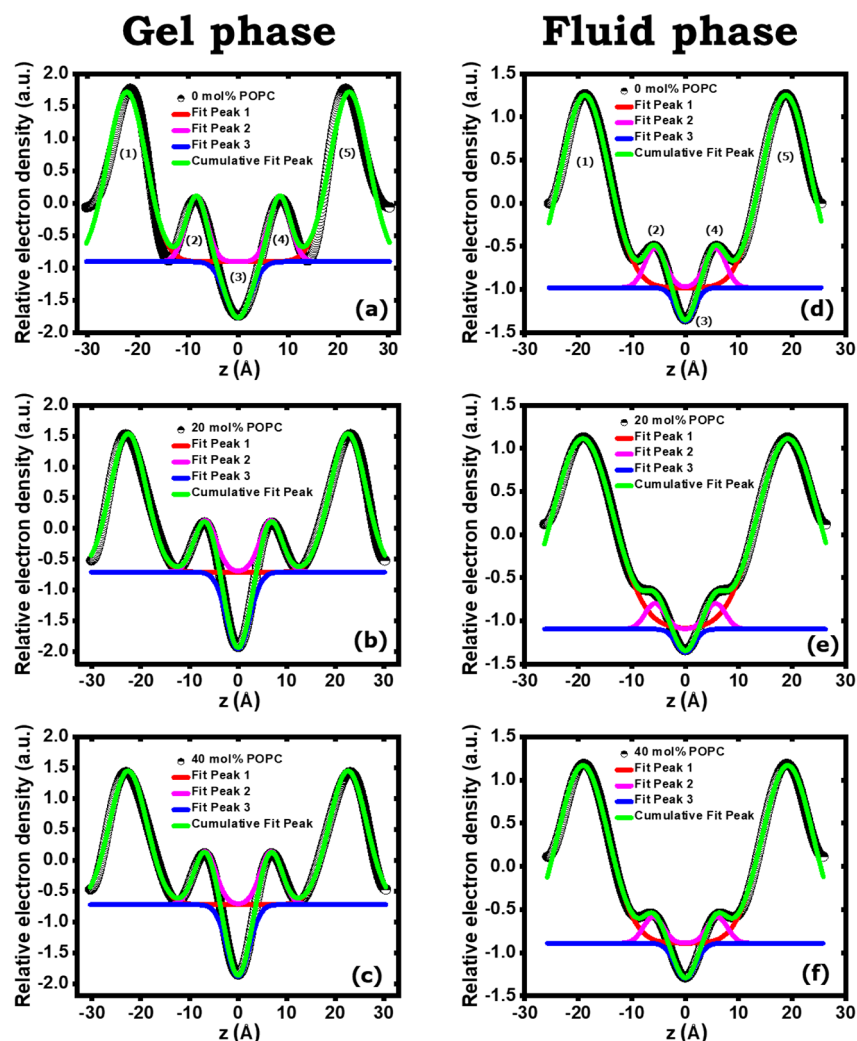


**Figure 6.** Electron density profiles (EDPs) fitted with an even function discussed in the text for the DPPC/DOPC system gel phase in the presence of (a) 0, (b) 20, and (c) 40 mol % POPC and fluid phase in the presence of (d) 0, (e) 20, and (f) 40 mol % of POPC. The black curve shows the EDP obtained using the swelling method described in the text, and the green curve shows the corresponding fit of the function.

**Table 1. Structural Parameters of the DPPC/DOPC (1:1) Membrane in the Presence of 0, 20, and 40 Mol % of POPC Determined by Fitting the Electron Density Profile Using an Even Function Discussed in the Text<sup>a</sup>**

sample	DPPC/DOPC/POPC = 50/50/0 mol %				DPPC/DOPC/POPC = 40/40/20 mol %				DPPC/DOPC/POPC = 30/30/40 mol %			
	gel phase $\rho_0 = -0.90 \pm 0.05$		fluid phase $\rho_0 = -0.98 \pm 0.02$		gel phase $\rho_0 = 0.71 \pm 0.01$		fluid phase $\rho_0 = -1.09 \pm 0.05$		gel phase $\rho_0 = -0.72 \pm 0.02$		fluid phase $\rho_0 = -0.89 \pm 0.03$	
parameters	$Z_n$ (Å)	$b_n$ (Å <sup>-2</sup> )	$Z_n$ (Å)	$b_n$ (Å <sup>-2</sup> )	$Z_n$ (Å)	$b_n$ (Å <sup>-2</sup> )	$Z_n$ (Å)	$b_n$ (Å <sup>-2</sup> )	$Z_n$ (Å)	$b_n$ (Å <sup>-2</sup> )	$Z_n$ (Å)	$b_n$ (Å <sup>-2</sup> )
$n = 1$ : peaks 1 & 5	$22.1 \pm 0.03$	$0.0339 \pm 0.0016$	$18.79 \pm 0.01$	$0.024 \pm 0.0001$	$22.59 \pm 0.01$	$0.0366 \pm 0.0001$	$19.1 \pm 0.01$	$0.015 \pm 0.0003$	$22.59 \pm 0.01$	$0.033 \pm 0.0002$	$19.13 \pm 0.01$	$0.022 \pm 0.0006$
$n = 2$ : peaks 2 & 4	$8.30 \pm 0.07$	$0.115 \pm 0.0124$	$5.63 \pm 0.04$	$0.1344 \pm 0.0117$	$6.75 \pm 0.07$	$0.096 \pm 0.0048$	$5.67 \pm 0.08$	$0.1477 \pm 0.0235$	$6.81 \pm 0.04$	$0.0998 \pm 0.0036$	$5.98 \pm 0.08$	$0.1418 \pm 0.0214$
$n = 3$ : trough 3	0	$0.0799 \pm 0.0108$	0	$0.1705 \pm 0.0179$	0	$0.0882 \pm 0.0062$	0	$0.1734 \pm 0.0297$	0	$0.0946 \pm 0.005$	0	$0.133 \pm 0.0157$

<sup>a</sup>The trough position at  $z = 0$  manifests the consideration of symmetric bilayer in the present analysis.

density distribution becomes symmetric about this  $z = 0$  Å as the analysis includes the mirror plane symmetry of the lipid bilayer. A detailed discussion can be found in previous publications.<sup>56,58,60</sup>

The main objective of this study, as explained above, is to investigate if there is any preferential participation of a hybrid lipid POPC in the domains of a mixed DPPC/DOPC system. The effect of POPC on XRR profile of the system obtained at 85% RH is shown in Figure 5 as a representative figure. The

data at other RHs are shown in Figure S1 along with the phasing and the continuous form factors at different lipid compositions in Figure S2 in the Supporting Information. The phase factors determined for the gel phase in the binary DPPC/DOPC system are  $[-1, -1, 1, -1, -1, 1]$  that change to  $[-1, -1, 1, -1, -1, -1]$  for the fluid phase. The EDPs obtained for both the gel and fluid phases in the presence of POPC in the DPPC/DOPC system are shown in Figure 6. The profile of the gel phase of the binary DPPC/DOPC

system is distinctly different from that of the fluid phase with a higher bilayer thickness. As reported earlier, the crystalline straight chains of the DPPC lipids form a thicker lipid layer compared to the DOPC with a random chain configuration at the measured temperature.<sup>60</sup>

For a better quantification of the structural parameters of each segment of the membrane, each electron density profile is then fitted using an even function given as

$$\rho(z) = \rho_0 + \sum_n \{ e^{-b_n(z-z_n)^2} + a_n e^{-b_n(z+z_n)^2} \} \quad (4)$$

where the function for  $n = 1$  fits the two peaks (1 and 5 in Figure 6) corresponding to the two head-groups of two opposing leaflets of the bilayer,  $n = 2$  fits the peaks representing the strongly interacted hydrocarbon chain regions (peaks 2 and 4), and  $n = 3$  for the inner core of the bilayer (trough 3). While  $z_n$  represents here the peak or trough position,  $b_n$  is related to the full width at half-maximum (FWHM) of the peak as

$\text{FWHM} = \frac{2\sqrt{2\ln 2}}{\sqrt{2b_n}}$ . Further, this FWHM can be considered as

the size of the relevant segment of the EDP. These two important parameters are tabulated in Table 1, which are used to quantify the changes in an EDP. Note that  $z_3 = 0$  signifies the trough position at the center of the bilayer about which the electron density of each leaflet is distributed symmetrically.  $\rho_0$  is the baseline taken for the cumulative fit, and  $a_n$  is the height of the  $n$ th peak. In the absence of POPC, the head-group size for DPPC-gel and DOPC-fluid phases is  $9.04 \pm 0.10$  and  $10.74 \pm 0.12$  Å, respectively, which are close to the reported values.<sup>60</sup>

The respective thickness of hydrocarbon chain regions is  $16.60 \pm 0.14$  and  $11.26 \pm 0.08$  Å obtained from  $d_{CC} = 2 \times z_2$ . With the addition of 20 mol % POPC, the head-group size decreases to  $8.70 \pm 0.04$  Å and increases to  $13.59 \pm 0.25$  Å for gel and fluid phases, respectively. These quantitative values suggest that the effect is much higher in the DOPC dominated fluid phase compared to the DPPC dominated gel one. The increased head-group size might be related to the relatively compact arrangement of lipids in the DOPC/POPC system compared to the DOPC dominated fluid phase. Such an arrangement may help in orienting the head-groups along the layer normal of the bilayer, providing a thicker layer. The bilayer thickness,  $d_{HH} = 2 \times z_1$ , excluding the water layer thickness, is the separation between two extreme head-groups symmetric about the middle portion of the EDP. According to our analysis, the  $d_{HH}$  value of DPPC is  $\sim 44.20 \pm 0.06$  Å and that of DOPC is  $\sim 37.58 \pm 0.02$  Å in the DPPC/DOPC (1:1) binary system. These values are consistent with the values reported in the literature.<sup>36,58,60,61</sup> With the addition of 20 mol % POPC in the membrane, there is an increase in the thickness to  $45.18 \pm 0.02$  and  $38.26 \pm 0.02$  Å for the gel and fluid phase, respectively. The increased thickness of the fluid phase is related to the physical presence of POPC in the bilayer. In such a case, one expects a relatively higher area fraction occupied by the DOPC phase in each bilayer. These larger regions in individual bilayer then will have better correlation across the bilayers. In turn, it should produce sharper XRR peaks presenting a longer correlation length. This is quantified and shown in the inset of Figure 5. This correlation length ( $L$ ) was calculated using the Scherrer formula:<sup>69,70</sup>

$L = \left( \frac{0.89 \times 2\pi}{\sqrt{(W_{\text{fit}})^2 - (\Delta q_{z,\text{reso}})^2}} \right)$ . Here  $W_{\text{fit}}$  is the full width at half-maximum (FWHM) of the Gaussian function fitted to the

reflection peak corresponding to a gel or fluid phase. The  $\Delta q_{z,\text{reso}}$  is the instrument resolution in  $q_z$  calculation. Note that the change in correlation length among the DPPC domains across the bilayers in the presence of POPC is much lower compared to the DOPC phase. As explained above, the thickness increase may happen for the gel phase due to a possible increase of the lateral pressure on the phase separated domains of DPPC lipids. Such a lateral pressure may decrease the chain tilt in the DPPC lipid, providing a slight increase in the bilayer thickness. This prediction is supported by the pressure–area isotherm measurements. A grazing incidence X-ray diffraction (GIXD) experiment, which produces Bragg peaks due to the in-plane organization of DPPC chains, may shed more light on this prediction. The formation of nanodomains in the presence of HLs in the mixture of saturated and unsaturated lipids has been reported earlier.<sup>30,71–75</sup> For such small domains, on the one hand, the line tension at the interface has to be reduced, and on other hand, the domains have to repel each other for their stability. Shimokawa et al. have discussed these issues in their work.<sup>32</sup> In the present study, even though these features have not been clearly quantified, it has quantified the preferential participation of the HL in the phase-separated domains. The phase behavior of POPC is very close to the behavior of DOPC at room temperature, which ensures the spontaneous mixing of these two lipids. The experimental techniques used here do not directly shed light on the organization of the HLs at the phase boundary; however, the weak structural effects on the gel phase of DPPC suggest such an arrangement. It is intuitive that the POPC lipids might have mixed in the DOPC domain homogeneously having a higher population at the phase boundary. Such a distribution may enhance the area fraction of the fluid phase reducing the size of the DPPC rich domain of the gel phase.

## 4. CONCLUSIONS

In the present study, isotherms of lipid monolayer and structure of lipid bilayer have been investigated to understand the preferential mixing of a hybrid lipid in a gel and fluid phase formed by a saturated and an unsaturated lipid, respectively. The thermodynamic parameters obtained from the isotherm measurements clearly showed that the hybrid lipid POPC mixes well in the unsaturated DOPC phase reducing the overall Gibbs free energy. The structural changes observed in the fluid phase are much more prominent compared to the gel phase, which are quantified by the electron density profile extracted from the X-ray reflectivity data. Further, the hybrid lipid POPC induces a bigger area fraction of DOPC by directly mixing in the fluid phase of the unsaturated lipid. On the other hand, even though there is no direct mixing of the hybrid lipid in the DPPC phase, its presence at the phase boundary changes the organization of the saturated lipid. However, the magnitude of this change is much weaker compared to the change in the unsaturated lipid phase.

## ■ ASSOCIATED CONTENT

### SI Supporting Information

The Supporting Information is available free of charge at <https://pubs.acs.org/doi/10.1021/acsoomega.1c04835>.

X-ray reflectivity (XRR) from lipid multilayers and phase factors of the mixed lipid system (PDF)

## AUTHOR INFORMATION

### Corresponding Author

Sajal K. Ghosh – Department of Physics, School of Natural Sciences, Shiv Nadar University, Gautam Buddha Nagar, Uttar Pradesh 201314, India; [orcid.org/0000-0002-4974-7311](https://orcid.org/0000-0002-4974-7311); Email: [sajal.ghosh@snu.edu.in](mailto:sajal.ghosh@snu.edu.in)

### Authors

Prashant Hitaishi – Department of Physics, School of Natural Sciences, Shiv Nadar University, Gautam Buddha Nagar, Uttar Pradesh 201314, India

Priya Mandal – Department of Physics, School of Natural Sciences, Shiv Nadar University, Gautam Buddha Nagar, Uttar Pradesh 201314, India

Complete contact information is available at:

<https://pubs.acs.org/10.1021/acsomega.1c04835>

### Notes

The authors declare no competing financial interest.

## ACKNOWLEDGMENTS

This research is financially supported by the Science & Engineering Research Board (SERB), Department of Science and Technology (DST), India, by funding the project (File EMR/2016/006221). We would like to thank Prof. Tim Salditt, University of Goettingen, and his group for the MATLAB tool used in analyzing the diffraction data. We also acknowledge the initial scientific discussions with Prof. Sunil K. Sinha, University of California-San Diego.

## REFERENCES

- (1) Singer, S. J.; Nicolson, G. L. The Fluid Mosaic Model of the Structure of Cell Membranes. *Science* **1972**, *175*, 720–731.
- (2) Mouritsen, O. G.; Bloom, M. Mattress Model of Lipid-Protein Interactions in Membranes. *Biophys. J.* **1984**, *46*, 141–153.
- (3) Simons, K.; Ikonen, E. Functional Rafts in Cell Membranes. *Nature* **1997**, *387*, 569–572.
- (4) Pike, L. J. Lipid Rafts: Bringing Order to Chaos. *J. Lipid Res.* **2003**, *44*, 655–667.
- (5) Pike, L. J. Rafts Defined: A Report on the Keystone Symposium on Lipid Rafts and Cell Function. *J. Lipid Res.* **2006**, *47*, 1597–1598.
- (6) Pike, L. J. The Challenge of Lipid Rafts. *J. Lipid Res.* **2009**, *50* Suppl, S323–S328.
- (7) Sezgin, E.; Levental, I.; Mayor, S.; Eggeling, C. The Mystery of Membrane Organization: Composition, Regulation and Roles of Lipid Rafts. *Nat. Rev. Mol. Cell Biol.* **2017**, *18*, 361–374.
- (8) Stöckl, M. T.; Herrmann, A. Detection of Lipid Domains in Model and Cell Membranes by Fluorescence Lifetime Imaging Microscopy. *Biochim. Biophys. Acta, Biomembr.* **2010**, *1798*, 1444–1456.
- (9) Nickels, J. D.; Smith, M. D.; Alsop, R. J.; Himbert, S.; Yahya, A.; Cordner, D.; Zolnierczuk, P.; Stanley, C. B.; Katsaras, J.; Cheng, X.; Rheinstädter, M. C. Lipid Rafts: Buffers of Cell Membrane Physical Properties. *J. Phys. Chem. B* **2019**, *123*, 2050–2056.
- (10) Veatch, S. L.; Keller, S. L. Separation of Liquid Phases in Giant Vesicles of Ternary Mixtures of Phospholipids and Cholesterol. *Biophys. J.* **2003**, *85*, 3074–3083.
- (11) McConnell, H. M.; Moy, V. T. Shapes of Finite Two-Dimensional Lipid Domains. *J. Phys. Chem.* **1988**, *92*, 4520–4525.
- (12) Almeida, P. F. F.; Pokorny, A.; Hinderliter, A. Thermodynamics of Membrane Domains. *Biochim. Biophys. Acta, Biomembr.* **2005**, *1720*, 1–13.
- (13) Lipowsky, R. Budding of Membranes Induced by Intra-membrane Domains. *J. Phys. II* **1992**, *2*, 1825–1840.
- (14) Brewster, R.; Pincus, P. A.; Safran, S. A. Hybrid Lipids as a Biological Surface-Active Component. *Biophys. J.* **2009**, *97*, 1087–1094.
- (15) Yamamoto, T.; Brewster, R.; Safran, S. A. Chain Ordering of Hybrid Lipids Can Stabilize Domains in Saturated/Hybrid/Cholesterol Lipid Membranes. *EPL* **2010**, *91*, 0–6.
- (16) Brewster, R.; Safran, S. A. Line Active Hybrid Lipids Determine Domain Size in Phase Separation of Saturated and Unsaturated Lipids. *Biophys. J.* **2010**, *98*, L21.
- (17) Yamamoto, T.; Safran, S. A. Line Tension between Domains in Multicomponent Membranes Is Sensitive to Degree of Unsaturation of Hybrid Lipids. *Soft Matter* **2011**, *7*, 7021–7033.
- (18) Bagatolli, L. A. Direct Observation of Lipid Domains in Free Standing Bilayers: From Simple to Complex Lipid Mixtures. *Chem. Phys. Lipids* **2003**, *122*, 137–145.
- (19) Haluska, C. K.; Schröder, A. P.; Didier, P.; Heissler, D.; Duportail, G.; Mély, Y.; Marques, C. M. Combining Fluorescence Lifetime and Polarization Microscopy to Discriminate Phase Separated Domains in Giant Unilamellar Vesicles. *Biophys. J.* **2008**, *95*, 5737–5747.
- (20) Celli, A.; Gratton, E. Dynamics of Lipid Domain Formation: Fluctuation Analysis. *Biochim. Biophys. Acta, Biomembr.* **2010**, *1798*, 1368–1376.
- (21) Veatch, S. L.; Keller, S. L. Organization in Lipid Membranes Containing Cholesterol. *Phys. Rev. Lett.* **2002**, *89*, 268101–268104.
- (22) Yuan, C.; Furlong, J.; Burgos, P.; Johnston, L. J. The Size of Lipid Rafts: An Atomic Force Microscopy Study of Ganglioside GM1 Domains in Sphingomyelin/DOPC/Cholesterol Membranes. *Biophys. J.* **2002**, *82*, 2526–2535.
- (23) Burgos, P.; Yuan, C.; Viriot, M. L.; Johnston, L. J. Two-Color near-Field Fluorescence Microscopy Studies of Microdomains (“Rafts”) in Model Membranes. *Langmuir* **2003**, *19*, 8002–8009.
- (24) Veatch, S. L.; Polozov, I. V.; Gawrisch, K.; Keller, S. L. Liquid Domains in Vesicles Investigated by NMR and Fluorescence Microscopy. *Biophys. J.* **2004**, *86*, 2910–2922.
- (25) Veatch, S. L.; Soubias, O.; Keller, S. L.; Gawrisch, K. Critical Fluctuations in Domain-Forming Lipid Mixtures. *Proc. Natl. Acad. Sci. U. S. A.* **2007**, *104*, 17650–17655.
- (26) Recktenwald, D. J.; McConnell, H. M. Phase Equilibria in Binary Mixtures of Phosphatidylcholine and Cholesterol. *Biochemistry* **1981**, *20*, 4505–4510.
- (27) Mills, T. T.; Huang, J.; Feigenson, G.; Nagle, J. Effects of cholesterol and unsaturated DOPC lipid on chain packing of saturated gel-phase DPPC bilayers. *Gen. Physiol. Biophys.* **2009**, *28*, 126.
- (28) McConlogue, C. W.; Vanderlick, T. K. A Close Look at Domain Formation in DPPC Monolayers. *Langmuir* **1997**, *13*, 7158–7164.
- (29) Jurak, M.; Mroczka, R.; Łopucki, R. Properties of Artificial Phospholipid Membranes Containing Lauryl Gallate or Cholesterol. *J. Membr. Biol.* **2018**, *251*, 277–294.
- (30) Feigenson, G. W. Phase Diagrams and Lipid Domains in Multicomponent Lipid Bilayer Mixtures. *Biochim. Biophys. Acta, Biomembr.* **2009**, *1788*, 47–52.
- (31) Szekely, O.; Schilt, Y.; Steiner, A.; Raviv, U. Regulating the Size and Stabilization of Lipid Raft-like Domains and Using Calcium Ions as Their Probe. *Langmuir* **2011**, *27*, 14767–14775.
- (32) Shimokawa, N.; Nagata, M.; Takagi, M. Physical Properties of the Hybrid Lipid POPC on Micrometer-Sized Domains in Mixed Lipid Membranes. *Phys. Chem. Chem. Phys.* **2015**, *17*, 20882–20888.
- (33) Salditt, T.; Li, C.; Spaar, A. Structure of Antimicrobial Peptides and Lipid Membranes Probed by Interface-Sensitive X-Ray Scattering. *Biochim. Biophys. Acta, Biomembr.* **2006**, *1758*, 1483–1498.
- (34) Tristram-Nagle, S. A. Preparation of Oriented, Fully Hydrated Lipid Samples for Structure Determination Using X-Ray Scattering. *Methods Mol. Biol.* **2007**, *400*, 63–75.
- (35) Tristram-Nagle, S.; Zhang, R.; Suter, R. M.; Worthington, C. R.; Sun, W. J.; Nagle, J. F. Measurement of Chain Tilt Angle in Fully

- Hydrated Bilayers of Gel Phase Lecithins. *Biophys. J.* **1993**, *64*, 1097–1109.
- (36) Mandal, P.; Bhattacharya, G.; Bhattacharyya, A.; Roy, S. S.; Ghosh, S. K. Unravelling the Structural Changes of Phospholipid Membranes in Presence of Graphene Oxide. *Appl. Surf. Sci.* **2021**, *539*, 148252.
- (37) Gupta, R.; Singh, A.; Srihari, V.; Ghosh, S. K. Ionic Liquid-Induced Phase-Separated Domains in Lipid Multilayers Probed by X-Ray Scattering Studies. *ACS Omega* **2021**, *6*, 4977–4987.
- (38) Giri, R. P.; Chakrabarti, A.; Mukhopadhyay, M. K. Cholesterol-Induced Structural Changes in Saturated Phospholipid Model Membranes Revealed through X-Ray Scattering Technique. *J. Phys. Chem. B* **2017**, *121*, 4081–4090.
- (39) Giri, R. P.; Mukhopadhyay, M. K.; Mitra, M.; Chakrabarti, A.; Sanyal, M. K.; Ghosh, S. K.; Bera, S.; Lurio, L. B.; Ma, Y.; Sinha, S. K. Differential Adsorption of a Membrane Skeletal Protein, Spectrin, in Phospholipid Membranes. *EPL* **2017**, *118*, 58002.
- (40) Hwang, M. J.; Kim, K. Poly(Ethylenimine) as a Subphase Stabilizer of Stearic Acid Monolayers at the Air/Water Interface: Surface Pressure-Area Isotherm and Infrared Spectroscopy Study. *Langmuir* **1999**, *15*, 3563–3569.
- (41) Datta, A.; Sanyal, M. K.; Dhanabalan, A.; Major, S. S. Formation of Highly Condensed Ferric Stearate Monolayers at the Air-Water Interface. *J. Phys. Chem. B* **1997**, *101*, 9280–9286.
- (42) Hao, C.; Zhang, L.; Zhang, Q.; Xu, G.; Sun, R. Effects of Hydrocarbon Chains Saturation Degree on Molecular Interaction between Phospholipids and Cholesterol in Mixed Monolayers. *Indian J. Biochem. Biophys.* **2017**, *54*, 186–190.
- (43) Giri, R. P.; Mukhopadhyay, M. K.; Basak, U. K.; Chakrabarti, A.; Sanyal, M. K.; Runge, B.; Murphy, B. M. Continuous Uptake or Saturation - Investigation of Concentration and Surface-Packing-Specific Hemin Interaction with Lipid Membranes. *J. Phys. Chem. B* **2018**, *122*, 7547–7554.
- (44) Bhattacharya, G.; Giri, R. P.; Dubey, A.; Mitra, S.; Priyadarshini, R.; Gupta, A.; Mukhopadhyay, M. K.; Ghosh, S. K. Structural Changes in Cellular Membranes Induced by Ionic Liquids: From Model to Bacterial Membranes. *Chem. Phys. Lipids* **2018**, *215*, 1–10.
- (45) Bhattacharya, G.; Mitra, S.; Mandal, P.; Dutta, S.; Giri, R. P.; Ghosh, S. K. Thermodynamics of Interaction of Ionic Liquids with Lipid Monolayer. *Biophys. Rev.* **2018**, *10*, 709–719.
- (46) Bakshi, K.; Mitra, S.; Sharma, V. K.; Jayadev, M. S. K.; Sakai, V. G.; Mukhopadhyay, R.; Gupta, A.; Ghosh, S. K. Imidazolium-Based Ionic Liquids Cause Mammalian Cell Death Due to Modulated Structures and Dynamics of Cellular Membrane. *Biochim. Biophys. Acta, Biomembr.* **2020**, *1862*, 183103.
- (47) Mitra, S.; Das, R.; Singh, A.; Mukhopadhyay, M. K.; Roy, G.; Ghosh, S. K. Surface Activities of a Lipid Analogue Room-Temperature Ionic Liquid and Its Effects on Phospholipid Membrane. *Langmuir* **2020**, *36*, 328–339.
- (48) Silvius, J. R. Thermotropic Phase Transitions of Pure Lipids in Model Membranes and Their Modifications by Membrane Proteins. *Lipid-protein Interact.* **1982**, *2*, 239–281.
- (49) Sabatini, K.; Mattila, J. P.; Kinnunen, P. K. J. Interfacial Behavior of Cholesterol, Ergosterol, and Lanosterol in Mixtures with DPPC and DMPC. *Biophys. J.* **2008**, *95*, 2340–2355.
- (50) Jurak, M. Thermodynamic Aspects of Cholesterol Effect on Properties of Phospholipid Monolayers: Langmuir and Langmuir-Blodgett Monolayer Study. *J. Phys. Chem. B* **2013**, *117*, 3496–3502.
- (51) Castillo, N.; Monticelli, L.; Barnoud, J.; Tieleman, D. P. Free Energy of WALP23 Dimer Association in DMPC, DPPC, and DOPC Bilayers. *Chem. Phys. Lipids* **2013**, *169*, 95–105.
- (52) Yang, S.-T.; Kiessling, V.; Tamm, L. K. Line Tension at Lipid Phase Boundaries as Driving Force for HIV Fusion Peptide-Mediated Fusion. *Nat. Commun.* **2016**, *7*, 1–9.
- (53) Palmieri, B.; Yamamoto, T.; Brewster, R. C.; Safran, S. A. Line Active Molecules Promote Inhomogeneous Structures in Membranes: Theory, Simulations and Experiments. *Adv. Colloid Interface Sci.* **2014**, *208*, 58–65.
- (54) Olżyńska, A.; Zubek, M.; Roeselova, M.; Korchowicz, J.; Cwiklik, L. Mixed DPPC/POPC Monolayers: All-Atom Molecular Dynamics Simulations and Langmuir Monolayer Experiments. *Biochim. Biophys. Acta, Biomembr.* **2016**, *1858*, 3120–3130.
- (55) Svetlovics, J. A.; Wheaton, S. A.; Almeida, P. F. Phase Separation and Fluctuations in Mixtures of a Saturated and an Unsaturated Phospholipid. *Biophys. J.* **2012**, *102*, 2526–2535.
- (56) Nagle, J. F.; Cognet, P.; Dupuy, F. G.; Tristram-Nagle, S. Structure of Gel Phase DPPC Determined by X-Ray Diffraction. *Chem. Phys. Lipids* **2019**, *218*, 168–177.
- (57) Pabst, G.; Kučerka, N.; Nieh, M. P.; Rheinstädter, M. C.; Katsaras, J. Applications of Neutron and X-Ray Scattering to the Study of Biologically Relevant Model Membranes. *Chem. Phys. Lipids* **2010**, *163*, 460–479.
- (58) Ghosh, S. K.; Aeffner, S.; Salditt, T. Effect of PIP2 on Bilayer Structure and Phase Behavior of DOPC: An X-Ray Scattering Study. *ChemPhysChem* **2011**, *12*, 2633–2640.
- (59) Ma, Y.; Ghosh, S. K.; Bera, S.; Jiang, Z.; Schlepütz, C. M.; Karapetrova, E.; Lurio, L. B.; Sinha, S. K. Anomalous Partitioning of Water in Coexisting Liquid Phases of Lipid Multilayers near 100% Relative Humidity. *Phys. Chem. Chem. Phys.* **2016**, *18*, 1225–1232.
- (60) Ma, Y.; Ghosh, S. K.; Dilena, D. A.; Bera, S.; Lurio, L. B.; Parikh, A. N.; Sinha, S. K. Cholesterol Partition and Condensing Effect in Phase-Separated Ternary Mixture Lipid Multilayers. *Biophys. J.* **2016**, *110*, 1355–1366.
- (61) Nagle, J. F.; Tristram-Nagle, S. Structure of Lipid Bilayers. *Biochim. Biophys. Acta - Rev. Biomembr.* **2000**, *1469*, 159–195.
- (62) Seul, M.; Sammon, M. J. Preparation of Surfactant Multilayer Films on Solid Substrates by Deposition from Organic Solution. *Thin Solid Films* **1990**, *185*, 287–305.
- (63) Sengupta, K.; Raghunathan, V. A.; Katsaras, J. Structure of the Ripple Phase of Phospholipid Multibilayers. *Phys. Rev. E - Stat. Physics, Plasmas, Fluids, Relat. Interdiscip. Top.* **2003**, *68*, 12.
- (64) Pabst, G.; Katsaras, J.; Raghunathan, V. A.; Rappolt, M. Structure and Interactions in the Anomalous Swelling Regime of Phospholipid Bilayers. *Langmuir* **2003**, *19*, 1716–1722.
- (65) King, G. L.; Jacobs, R. E.; White, S. H. Hexane Dissolved in Dioleoyllecithin Bilayers Has a Partial Molar Volume of Approximately Zero. *Biochemistry* **1985**, *24*, 4637–4645.
- (66) Karmakar, S.; Raghunathan, V. A. Structure of Phospholipid-Cholesterol Membranes: An x-Ray Diffraction Study. *Phys. Rev. E - Stat. Nonlinear, Soft Matter Phys.* **2005**, *71*, 1–10.
- (67) Raghunathan, V. A.; Katsaras, J. Structure of the  $L_c$  phase in a hydrated lipid multilamellar system. *Phys. Rev. Lett.* **1995**, *74*, 4456.
- (68) Blaurock, A. E. Structure of the Nerve Myelin Membrane: Proof of the Low-Resolution Profile. *J. Mol. Biol.* **1971**, *56*, 35–52.
- (69) Scherrer, P. Bestimmung Der Inneren Struktur Und Der Größe von Kolloidteilchen Mittels Röntgenstrahlen. *Kolloidchem. Ein Lehrb.* **1912**, *387*–409.
- (70) Patterson, A. L. The Scherrer Formula for X-Ray Particle Size Determination. *Phys. Rev.* **1939**, *56*, 978.
- (71) Heberle, F. A.; Petruzielo, R. S.; Pan, J.; Drazba, P.; Kučerka, N.; Standaert, R. F.; Feigenson, G. W.; Katsaras, J. Bilayer Thickness Mismatch Controls Domain Size in Model Membranes. *J. Am. Chem. Soc.* **2013**, *135*, 6853–6859.
- (72) Pathak, P.; London, E. The Effect of Membrane Lipid Composition on the Formation of Lipid Ultrananodomains. *Biophys. J.* **2015**, *109*, 1630–1638.
- (73) Pathak, P.; London, E. Measurement of Lipid Nanodomain (Raft) Formation and Size in Sphingomyelin/POPC/Cholesterol Vesicles Shows TX-100 and Transmembrane Helices Increase Domain Size by Coalescing Preexisting Nanodomains but Do Not Induce Domain Formation. *Biophys. J.* **2011**, *101*, 2417–2425.
- (74) Heberle, F. A.; Wu, J.; Goh, S. L.; Petruzielo, R. S.; Feigenson, G. W. Comparison of Three Ternary Lipid Bilayer Mixtures: FRET and ESR Reveal Nanodomains. *Biophys. J.* **2010**, *99*, 3309–3318.
- (75) Hassan-Zadeh, E.; Baykal-Caglar, E.; Alwarawrah, M.; Huang, J. Complex Roles of Hybrid Lipids in the Composition, Order, and Size of Lipid Membrane Domains. *Langmuir* **2014**, *30*, 1361–1369.